Reaction Kinetics, Mechanisms and Catalysis (2023) 136:1819–1837
https://doi.org/10.1007/s11144-023-02465-1

Kinetic evaluation for the reaction of hydroxylamine with acetamide using online infrared spectra and pH profile analysis

Jialei Jin[1] · Liwei Ni[1] · Wenze Qiu[1] · Qiyue Xu[1] · Shuliang Ye[1]

Received: 10 April 2023 / Accepted: 3 August 2023 / Published online: 14 August 2023

Abstract

In this study, the reaction of hydroxylamine with acetamide to acetohydroxamic acid was carried out at different temperatures, and the complete reaction processes were monitored using online infrared spectroscopy and pH probe. Regarding the reaction as first-order for both reactants, the obtained experimental data were fitted to evaluate kinetic parameters, including the second-order rate constant k of the reaction at different temperatures, and the activation energy E_A. It was found that when fitting online infrared spectral data, the traditional hard-modeling method was not able to obtain reasonable evaluated values of kinetic parameters due to the influence of rotation ambiguity. In this study, spectral similarity was innovatively applied to restrain the rotational ambiguity during IR spectra fitting and has achieved favorable effects. The values of the apparent dissociation constants of weak acidic or basic substances in the reaction model were additionally evaluated during online pH profile fitting. In addition, a multi-objective optimization method, NSGA-II, was also carried out to fit online IR spectra and pH profile simultaneously. The E_A evaluation results obtained by the three mentioned methods were similar, with values of 85.10, 84.48, and 83.72 kJ mol^{-1}, while the multi-objective optimization method provided evaluation results for the rate constant k with the smallest relative standard deviation (maximum 5.72%).

Keywords Online infrared spectroscopy · Online pH profile · Kinetic model parameter fitting · Rate constant · Multi-objective optimization

✉ Shuliang Ye
itmt_paper@126.com

[1] Institute of Industry and Trade Measurement Technology, China Jiliang University, Hangzhou 310018, China

Introduction

Acetohydroxamic acid is widely used in agriculture, medical, and environment protection fields [1]. One of the common procedures for the synthesis of acetohydroxamic acid involves the reaction between hydroxylamine and acetamide [2]. In order to efficiently control and optimize such a procedure, it is essential to comprehend the kinetics of this reaction. Chemical reaction kinetics provide a quantitative measurement of the rates of reactions and provide insight into the influencing factors of reaction rates, such as concentration, temperature, pressure, and catalysts. Establishing a proper reaction model with precise reaction parameters (such as rate constants, activation energies, and reaction orders) is critical for controlling a reaction for the desired outcome.

The experimental determination of reaction kinetic parameters often involves measuring the concentrations changes of reactants or products during the reaction process, or at least signals that correlate with the turnover of reactants to products. Various monitoring instruments meeting the above requirement have been used for chemical reaction kinetic analysis. These instruments can be divided into two groups by their monitoring method: offline monitoring and online monitoring.

Although the offline monitoring instruments can distinguish the components in the mixture, they suffer from limited time resolution, potential sample contamination, and the inability to capture transient species accurately [3, 4]. By comparison, online monitoring technologies, such as online infrared spectroscopy, online UV–visible spectroscopy, online Raman spectroscopy, and reaction calorimetry, seem to be better choices to acquire kinetic data [5–9]. These techniques enable continuous and real-time monitoring of the reaction progress, providing detailed information on reaction progress. Besides, by directly probing the reaction mixture without the need for manual sampling, online measurements reduce the risk of sample contamination and preserve the integrity of the reaction system, and have been increasingly used in the kinetic analysis of the reaction process.

Among the various online monitoring technologies used for kinetic analysis, online infrared spectroscopy stands out as a commonly used approach as the interpretation of the results is generally straightforward [10]. Its broad wavenumber range enables the identification of diverse chemical bonds and functional groups, and the absorbance correlates with the concentration of detected substances. The widely used kinetic parameter evaluation method based on online infrared spectra is referred to as the 'hard-modeling' method. It directly uses the spectral data set of the entire reaction as the fitting object and evaluates the kinetic parameters during the fitting process. This approach is calibration-free and does not require the establishment of a quantitative model [11–14]. The traditional hard-modeling approach, however, is easily affected by rotational ambiguity and leads to erroneous fitting results [14–17]. In this study, we tried to restrain the adverse effect of rotational ambiguity on the parameter fitting by introducing the similarity between the calculated pure spectra and the measured ones into the objective function of the fitting process.

Facile access to utilize a variety of online monitoring techniques allows for the simultaneous use of more than one such technique in numerous cases, and

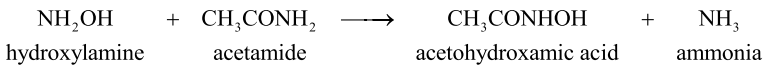

Scheme 1 Acetohydroxamic acid synthesis

multiple techniques can mutually validate or complement each other [4]. Carvalho et al. [18] monitored a second-order reaction between benzophenone and phenylhydrazine using online UV/vis and mid-infrared spectroscopic probes and obtained consistent rate constant evaluation results from the independent analysis of both types of data. Chung et al. [19] applied tandem online infrared spectroscopy and offline HPLC–MS to monitor the dysprosium (III) triflate-catalyzed aza-Piancatelli rearrangement of 2-furylcarbinols. The offline HPLC revealed the formation of a transient intermediate that was not visualized in the IR data. However, neither of these studies has demonstrated the idea of combining different types of data and analyzing them together in a same calculation process.

In this study, an online pH probe was combined with the online infrared spectrometer for reaction monitoring, given its simple operation, and the correlation between pH changes and variations in the concentrations of acidic or basic substances in the system. A commonly used multi-objective fitting algorithm, Non-dominated Sorting Genetic Algorithm II (NSGA-II) [20], was used to evaluate experimental data of infrared and pH simultaneously, in order to improve the accuracy of evaluation results. The results demonstrated the feasibility of this method in improving the accuracy and stability of the evaluation results.

Materials and methods

Reaction

The reaction of hydroxylamine and acetamide that synthesize acetohydroxamic acid (Scheme 1) [21, 22] was studied here.

The reaction was carried out using a molar ratio of 1:1 hydroxylamine to acetamide. As one of the reactants, hydroxylamine was prepared by dissolving a calculated amount of hydroxylamine hydrochloride and NaOH in 50 mL deionized water. In order to ensure that the pH change caused by the concentration changes of weak acidic or basic substances during the synthesis of acetohydroxamic acid can be observed, the NaOH amount (5.70 g, 0.14 mol) was slightly less than hydroxylamine hydrochloride (10.43 g, 0.15 mol) to ensure the complete consumption of NaOH. 8.86 g acetamide was then put into the prepared hydroxylamine solution as another reactant to generate acetohydroxamic acid and ammonia.

Experimental setup

Isothermal batch experiments were carried out separately at 55, 50, 45, 40, and 35 °C. For each temperature, the experiment was repeated three times to validate

the repeatability of the experiment, and each experiment was terminated after 5 h of reaction. The reactor was sealed during the reaction process. The reaction process was monitored by an online FTIR spectrometer (ReactIR-702L, Mettler Toledo, USA) and an online pH probe (SIN-PH-6002, Sinomeasure, China) simultaneously. The infrared spectra were collected with a resolution of 2 cm^{-1} and a sampling interval of 15 s. The pH data were recorded every 5 s.

The pH probe has automatic temperature compensation function and was calibrated with calibration buffers of known pH values before each experiment. The infrared spectrum of the solvent water was measured before adding the reactants and used as the background, which was subtracted from the raw reaction spectra. The processed infrared spectra were then evaluated in the range of 1800–850 cm^{-1}, and formed the matrix $\mathbf{D}_{exp}$, while the pH data were concatenated to a single vector $\mathbf{pH}_{exp}$.

Establishment of reaction kinetic model

In order to simplify the calculation process, the synthesis reaction of acetohydroxamic acid was considered as a second-order reaction overall, and first-order with respect to each reactant [22]. In addition, according to the description in the reference [22], there is no accumulation of any additional intermediate that can be observed by infrared spectrometer in the reaction process (our experimental results also proved this). Therefore, the kinetic model can be described by the following equations [23]:

$$\begin{gathered}
\mathrm{NH_2OH + CH_3CONH_2 \xrightarrow{k} CH_3CONHOH + NH_3} \\
\mathrm{A + B \xrightarrow{k} P} \\
r(k) = k \cdot c_{\mathrm{A}} \cdot c_{\mathrm{B}} \\
\frac{\mathrm{d}c_{\mathrm{A}}}{\mathrm{d}t} = -r(k) \\
\frac{\mathrm{d}c_{\mathrm{B}}}{\mathrm{d}t} = -r(k) \\
\frac{\mathrm{d}c_{\mathrm{P}}}{\mathrm{d}t} = r(k).
\end{gathered} \tag{1}$$

It needs to be emphasized that since acetohydroxamic acid and ammonia were generated synchronously and in the same amount, they are both represented by the component P in the kinetic model, while A and B represent hydroxylamine and acetamide separately. c_A, c_B, and c_P are the concentrations of the corresponding substances in the solvent (mol L^{-1}). $r(k)$ is the reaction rate (mol L^{-1} s^{-1}), which is proportional to the product of the concentrations of the reactants. The proportional constant k (L mol^{-1} s^{-1}) is the isothermal rate constant of the reaction and is the only unknown parameter of the reaction kinetic model.

Evaluation of the rate constant using online IR spectra

According to the Beer-Lambert law, the reaction spectrum (matrix **D**) can be decomposed into the pure spectra of all absorbing chemical components of the reaction mixture (matrix **S**) and their corresponding concentration–time profiles (matrix **C**) (Eq. 2) [24]:

$$\mathbf{D} = \mathbf{CS} + \mathbf{E} \tag{2}$$

The matrix **E** describes the matrix of residuals that cannot be explained by the resolved components including the random noises.

A reasonable and unique decomposition is only possible if appropriate physical constraints are applied. Here the measured reaction spectrum $\mathbf{D}_{exp}$ was decomposed using a specified kinetic model with unknown parameters as a physical constraint for the concentration–time profiles, which is called the hard-modeling approach [16, 25]. The parameters of the kinetic model can be evaluated directly through the decomposition process. This so-called hard-modeling approach can be roughly divided into the following three steps: First, the concentration matrix $\mathbf{C}_{calc}(k)$ is calculated according to the kinetic model. Second, the complete matrix of pure component spectra $\mathbf{S}_{calc}$ is calculated by linear least squares (Eq. 3):

$$\mathbf{S}_{calc} = \mathbf{C}_{calc}(k)^{+}\mathbf{D}_{exp} \tag{3}$$

Here $\mathbf{C}_{calc}(k)^{+}$ represents the pseudo inverse matrix of $\mathbf{C}_{calc}(k)$. Third, a nonlinear optimization was conducted with an objective function F_{IR} as Eq. 4:

$$F_{IR} = \left\| \mathbf{D}_{exp} - \mathbf{C}_{calc}(k)\mathbf{S}_{calc} \right\| \tag{4}$$

and the calculation restarts at step one. The optimization process was conducted with Matlab using the lsqnonlin function for the nonlinear least square optimization.

The fitting of the rate constant k is completed simultaneously in the decomposition process by constantly adjusting the given value of the parameter during the iterative process until the objective function reaches the minimum value. The nonlinear optimization process requires specifying the initial value of the kinetic parameter to start.

It should be noted that the decomposition of the infrared spectra is easily affected by the rotational ambiguity, and even if the kinetic model has been added as a constraint, it may still lead to inappropriate results. See Supplementary Information for more details. Therefore, in this study, we propose a method that involves comparing the decomposition results $\mathbf{S}_{calc}$ with the measured spectra of pure substances and treating the similarity between them as an additional part of the iterative objective function. This approach aims to add a further physical constraint into the fitting process.

The vectors of difference between calculated and measured spectra are combined with $\mathbf{D}_{exp} - \mathbf{C}_{calc}(k)\mathbf{S}_{calc}$ to form a new matrix, and the objective function F_{IR} is now changed to Eq. 5:

$$F_{\mathrm{IR}} = \left\| \begin{bmatrix} \mathbf{D}_{\mathrm{exp}} - \mathbf{C}_{\mathrm{calc}}(k)\mathbf{S}_{\mathrm{calc}} \\ \mathbf{S}_{\mathrm{exp},1} - \mathbf{S}_{\mathrm{calc},1} \\ \vdots \\ \mathbf{S}_{\mathrm{exp},l} - \mathbf{S}_{\mathrm{calc},l} \\ \vdots \end{bmatrix} \right\| \tag{5}$$

Here different l represents different substances, whose measured pure spectra can be obtained. For the synthesis of acetohydroxamic acid, the spectra of hydroxylamine, acetamide, and product were measured (scaled according to the concentration of the corresponding component in a pure liquid) and compared with the decomposition results.

Note that measured spectra of pure components have been utilized in the optimization process in other studies [16, 26, 27], but they were directly used to replace the corresponding line of $\mathbf{S}_{\mathrm{calc}}$ in the objective function. However, due to the influence of other substances and external conditions, the spectrum of the substance in the reaction system may differ from the one measured from the pure substance [15]. Therefore, simply replacing $\mathbf{S}_{\mathrm{calc}}$ with measured pure spectra may not achieve the desired effect, as will be further discussed in Sect. "Fitting results of online IR spectra" below. In comparison, using the similarity of the calculated and measured spectra as a part of the optimized function seems to be a more flexible method to improve the creditability of the decomposition process.

Evaluation of the rate constant using online pH profile

The fitting process of pH data is similar to that of infrared data, except that the objective function changes to $F_{\mathrm{pH}} = \left\| \mathbf{pH}_{\mathrm{exp}} - \mathbf{pH}_{\mathrm{calc}} \right\|$. Therefore, before introducing the evaluation process of the rate constant based on the pH profile, it is necessary to introduce the simulation method for calculating the pH profile of the reaction process which forms the vector $\mathbf{pH}_{\mathrm{calc}}$.

Simulation of pH profile of reaction process

During the synthesis reaction of acetohydroxamic acid, the acidic and basic substances that affect the pH value include hydroxylamine, acetohydroxamic acid, and ammonia. These substances are weak electrolytes and have ionization equilibrium processes in aqueous solutions as same as water molecules. Their ionization equilibrium equations and ionization equilibrium constants (*Ka* for acid, and *Kb* for base) are expressed as follows [28–31]:

$$\begin{aligned} &\mathrm{NH_2OH} + \mathrm{H_2O} \overset{Kb_{\mathrm{NH_2OH}}}{\rightleftharpoons} \mathrm{NH_3OH^+} + \mathrm{OH^-} \\ &Kb_{\mathrm{NH_2OH}} = \left[\mathrm{NH_3OH^+}\right]\left[\mathrm{OH^-}\right] / \left[\mathrm{NH_2OH}\right] \end{aligned} \tag{6}$$

$$\begin{gathered} \mathrm{CH_3CONHOH} + \mathrm{H_2O} \overset{Ka_{\mathrm{CH_3CONHOH}}}{\rightleftharpoons} \mathrm{CH_3CONOH^-} + \mathrm{H_3O^+} \\ Ka_{\mathrm{CH_3CONHOH}} = \left[\mathrm{CH_3CONOH^-}\right]\left[\mathrm{H^+}\right] / \left[\mathrm{CH_3CONHOH}\right] \end{gathered} \tag{7}$$

$$\begin{gathered} \mathrm{NH_3} + \mathrm{H_2O} \overset{Kb_{\mathrm{NH_3}}}{\rightleftharpoons} \mathrm{NH_4^+} + \mathrm{OH^-} \\ Kb_{\mathrm{NH_3}} = \left[\mathrm{NH_4^+}\right]\left[\mathrm{OH^-}\right] / \left[\mathrm{NH_3}\right] \end{gathered} \tag{8}$$

$$\begin{gathered} \mathrm{H_2O} \overset{K_W}{\rightleftharpoons} \mathrm{H^+} + \mathrm{OH^-} \\ K_W = \left[\mathrm{H^+}\right]\left[\mathrm{OH^-}\right] \end{gathered} \tag{9}$$

Here [X] is the concentration of the substance X (mol L^{-1}).

The pH of the reaction system can be calculated according to the charge balance equation [32–34]:

$$\left[\mathrm{H^+}\right] + \left[\mathrm{NH_3OH^+}\right] + \left[\mathrm{NH_4^+}\right] + \left[\mathrm{Na^+}\right] = \left[\mathrm{OH^-}\right] + \left[\mathrm{Cl^-}\right] + \left[\mathrm{CH_3CONOH^-}\right] \tag{10}$$

Here Na^+ and Cl^- were introduced by NaOH and hydroxylamine hydrochloride when generating hydroxylamine.

Meanwhile, based on the conservation law of atoms, the following equation also exists in the system:

$$\left[\mathrm{NH_3OH^+}\right] + \left[\mathrm{NH_2OH}\right] = C_{\mathrm{NH_2OH}} \tag{11}$$

$$\left[\mathrm{CH_3CONHOH}\right] + \left[\mathrm{CH_3CONOH^-}\right] = C_{\mathrm{CH_3CONHOH}} \tag{12}$$

$$\left[\mathrm{NH_3}\right] + \left[\mathrm{NH_4^+}\right] = C_{\mathrm{NH_3}} \tag{13}$$

Combining Eqs. 6, 7, 8, 9, 10, 11, 12 and 13 then Eq. 10 can be converted into the form below:

$$\begin{aligned} &\frac{K_W}{\left[\mathrm{OH^-}\right]} + C_{\mathrm{NH_2OH}} \cdot \frac{Kb_{\mathrm{NH_2OH}}}{Kb_{\mathrm{NH_2OH}} + \left[\mathrm{OH^-}\right]} + \left[\mathrm{Na^+}\right] + C_{\mathrm{NH_3}} \cdot \frac{Kb_{\mathrm{NH_3}}}{Kb_{\mathrm{NH_3}} + \left[\mathrm{OH^-}\right]} \\ &= \left[\mathrm{OH^-}\right] + \left[\mathrm{Cl^-}\right] + C_{\mathrm{CH_3CONHOH}} \cdot \frac{Ka_{\mathrm{CH_3CONHOH}}}{\frac{K_W}{\left[\mathrm{OH^-}\right]} + Ka_{\mathrm{CH_3CONHOH}}} \end{aligned} \tag{14}$$

Here $[Na^+]$ is the feed amount of NaOH (mol L^{-1}) and $[Cl^-]$ is the one of hydroxylamine hydrochloride (mol L^{-1}), both of which are known. The concentrations C of other substances change during the reaction and can be calculated with the kinetic model. Therefore, if all ionization equilibrium constants are known, the above equation becomes a unary equation about $[OH^-]$, and the value of $[OH^-]$ can be calculated by solving the equation.

The calculated value of pH can then be obtained by Eq. 15:

$$\mathrm{pH} = -\log\left(K_W\right) + \log\left([\mathrm{OH}^-]\right) \tag{15}$$

Here K_W is the ionization constant of water, which has different values at different temperatures, and the specific values used in this study were referenced from [35].

In order to simplify the pH calculation process, the influence of activity coefficients of each component on the dissociation constants [34, 36] is neglected. Therefore, we refer to the dissociation constants involved in the calculation process as apparent dissociation constants [36, 37]. From the subsequent discussion of the calculation results, it can be seen that such neglect does not seem to have a great impact on the fitting results of the kinetic model parameters, thus it should be feasible.

Evaluation of the rate constant

As described previously, if $C_{\mathrm{NH_2OH}}$,$C_{\mathrm{NH_3}}$,$C_{\mathrm{CH_3CONHOH}}$, and all apparent dissociation constants are known, the pH of the reaction process can be calculated by Eqs. 14 and 15, and the values of $C_{\mathrm{NH_2OH}}$,$C_{\mathrm{NH_3}}$, and $C_{\mathrm{CH_3CONHOH}}$ can be calculated by the kinetic model. Although the dissociation constants of various substances can be found in the literature, their values may not be applicable here due to the influence of temperature and other existing components. Therefore, in this study, the apparent dissociation constants are taken as unknown parameters to be fitted in the optimization process, as well as the rate constant k of the kinetic model. The identification process of unknown parameters based on the pH profile of the reaction process can be summarized as follows:

Step 1: A set of initial values of the rate constant k and the apparent dissociation constants of each weak acidic or basic substance are given, and the value range of each parameter is specified to start the nonlinear iterative optimization process.

Step 2: $\mathbf{C}_{\mathrm{calc}}(k)$ is calculated based on the kinetic model and the value of k.

Step 3: The values of $C_{\mathrm{NH_2OH}}$, $C_{\mathrm{NH_3}}$ and $C_{\mathrm{CH_3CONHOH}}$ at different times are taken from the corresponding columns of $\mathbf{C}_{\mathrm{calc}}(k)$, and $\mathbf{pH}_{\mathrm{calc}}(k, Ka_i, Kb_i)$ is calculated through Eqs. 14 and 15.

Step 4: An objective function $F_{\mathrm{pH}}=\left\|\mathbf{pH}_{\mathrm{exp}} - \mathbf{pH}_{\mathrm{calc}}\right\|$ is fed to the nonlinear optimization, and the optimization algorithm will suggest new estimates for the rate constant k and the apparent dissociation constants ($Kb_{\mathrm{NH_2OH}}$, $Ka_{\mathrm{CH_3CONHOH}}$, and $Kb_{\mathrm{NH_3}}$). The calculation then restarts at step 2 until a minimum F_{pH} is found. The optimization process was conducted with Matlab using the lsqnonlin function for the nonlinear least square optimization.

The fitting of the pH profile not only reveals the kinetic model parameters but also obtains the values of the apparent dissociation constants of weak acidic or basic substances in the reaction model as additional results. The fitting of the pH profile does not involve the problem of rotational ambiguity. As long as the measurement of pH is accurate and the established pH model is comprehensive, the only result with physical significance can be obtained.

Evaluation of the rate constant using muli-objective fitting

NSGA-II for finding pareto-optimal set

Note that both parameter evaluation methods mentioned above are based on fitting a single type of experimental data, to further analyze the experiment and fuse the data collected from the two sensors, a multi-objective optimization algorithm, NSGA-II, is executed to fit IR and pH experimental data simultaneously. The concept of NSGA-II is based on the non-dominated sorting and elitist selection theory [20, 38]. For the specific calculation process of NSGA-II, please refer to Reference [20].

When NSGA-II terminates, it will obtain a set of non-dominated solutions known as the Pareto optimal set. This set contains a group of solutions in a multi-objective optimization problem that cannot be improved in any one objective without worsening another [39]. The corresponding objective function values of the Pareto optimal set form the Pareto frontier. In this study, there were two objective functions, F_{IR} and F_{pH}, to be minimized, representing the fitting error of infrared and pH data. Each solution consisted of a set of evaluation values for the model parameters, including the rate constant k and the apparent dissociation constants of each weak acidic or basic substance. The multi-objective optimization process was conducted with Matlab using the gamultiobj function.

Weighted sum method (WSM) for finding the optimal solution among the pareto optimal set

The resolution of a multi-objective optimization problem does not end when the Pareto optimal set is found. In practical applications, a single solution must be selected from the Pareto frontier [40]. The selection of the optimal solution involves a multi-criteria decision making (MCDM) problem [41], where the non-dominated solutions of the Pareto frontier and the objective function of optimization are redefined as alternatives and criteria of the MCDM problem.

The weighted sum method was used to select the final optimal solution from the Pareto optimal set. As one of the most widely used MCDM methods, WSM is based on the assumption of independent values of an attribute from each other. See Eqs. S2-S9 in the Supplementary Information for the specific calculation process of WSM.

Evaluation of the activation energy

According to the Arrhenius equation, the relationship between temperatures and rate constants k is as follows [42]:

$$\ln(k) = \ln(A) - \frac{E_A}{\mathrm{R}T} \tag{16}$$

where k is the reaction rate constant at temperature T(K); A is the pre-exponential factor, which is a constant; E_A (kJ mol^{-1}) is the activation energy of the reaction; R is the molar gas constant. Therefore, there exists a linear relationship between ln(k) and 1/T with a slope of $-E_A$/R. Once the rate constants for each reaction temperature are obtained, a linear regression can be performed on the logarithm (base e) of these values, then the activation energy can be calculated based on the slope of the linear equation.

Results and discussion

Experimental results

Fig. 1 shows the infrared spectra obtained by sampling every half hour from three replicates of the reaction progress at 55 °C and averaging the results. See Fig. S1 for the infrared spectra of the reaction processes at other temperatures.

The characteristic peaks in Fig. 1 are highlighted, where the intensity of absorption peak at around 1184 cm^{-1} gradually decreased, which belongs to the -NH_2 wagging vibration of hydroxylamine according to the literature [43]. The absorption peaks at around 1090 and 988 cm^{-1} gradually increased, and both of them may correspond to the vibration of –CH_3 and N–O groups in acetohydroxamic acid according to the literature [44]. A point with no change in absorption throughout the reaction process is observed in the infrared spectra (Fig. 1). This point is referred to as an isosbestic point, and is good evidence of a reaction without the accumulation of intermediates, because isosbestic points will be lost if changes in reaction conditions occur, such as temperature variations during the reaction or presence of an intermediate [18].

Fig. 2 shows the characteristic profiles that can represent the reaction progress, and the influence of temperature on the reaction rate can be seen in all four panels. In Fig. 2a, the characteristic peak absorbance of the reactant decreases more rapidly with increasing reaction temperature, while in Fig. 2b, the characteristic peak absorbance of the product shows an accelerated increase with rising reaction temperature. Fig. 2c

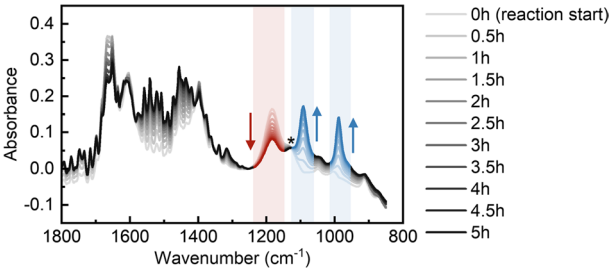

Fig. 1 Online IR spectra of acetohydroxamic acid synthesis reaction at 55 °C (the average of three repeated experiments). The peak at around 1184 cm^{-1} belongs to the reactant, and shows a falling trend as the reaction proceeds, while the peaks at around 1090 and 988 cm^{-1} belong to the product, and show rising trends as the reaction proceeds. The mark (*) shows the isosbestic point

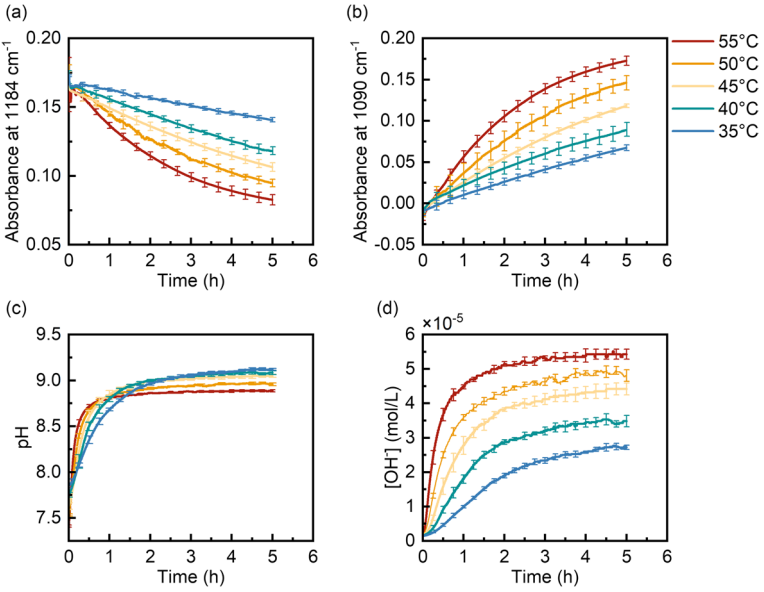

Fig. 2 Characteristic profiles of reaction process at 55, 50, 45, 40, and 35 °C. All profiles only show the part after the start of the reaction, and the start time of each reaction was set to zero for comparison: **a** the absorbance-time profile at 1184 cm^{-1} extracted from online IR spectra; **b** the absorbance-time profile at 1090 cm^{-1} extracted from online IR spectra; **c** the pH-time profile measured by online pH probe; **d** the concentration of OH^--time profile calculated by Eq. 15. The error bars were determined by the experimental repeats mentioned in Sect. "Experimental setup"

shows the pH profiles of the reaction process at different temperatures. The increasing temperature leads to a faster pH change of the system, and this effect can be seen more clearly in Fig. 2d, where the pH is converted to the concentration of OH^- in the system using Eq. 15.

According to Fig. 2c, the pH of the reaction process changed within the range of 7.5 to 9.5, and the system basically remained in a weak basic environment. Therefore, it was assumed that the change in pH did not significantly impact the rate constant, and the pH profile was used as another fitting object for the kinetic parameter evaluation of the acetohydroxamic acid synthesis reaction, in addition to the online infrared spectral data.

The data obtained from each experiment were separately fitted to obtain the evaluated kinetic parameters. The mean and standard deviation of the parameter evaluation results at the same temperature were summarized in Tables 1, 2 and 3. For detailed parameter evaluation results of each experiment and the goodness of fit of the kinetic model to the experimental data, refer to Tables S1–S3.

Table 1 Evaluated values of rate constant k at different temperatures obtained by fitting the online IR spectra using nonlinear least square optimization method with different objective function

Temperature (°C)	Rate constant k (10^{-5} L mol^{-1} s^{-1})		
	Method A[a]	Method B[b]	Method C[c]
55	2.867 ± 1.100	6.217 ± 3.410	6.896 ± 0.571
50	2.335 ± 0.863	3.589 ± 0.383	3.947 ± 0.091
45	3.049 ± 2.828	4.025 ± 2.941	2.243 ± 0.180
40	6.069 ± 1.709	2.323 ± 0.601	1.573 ± 0.068
35	3.357 ± 5.267	2.898 ± 1.638	0.862 ± 0.090

[a]Method *A*: traditional hard-modeling approach where the objective function of the fitting process is Eq. 4

[b]Method *B*: directly replacing the corresponding rows in $\mathbf{S}_{calc}$ with the measured pure spectra in the fitting process

[c]Method *C*: introducing the similarity between the calculated and measured pure spectra into the objective function of the fitting process, and changing the objective function to Eq. 5

Table 2 Evaluated values of rate constant k and apparent dissociation constants of substances at different temperatures obtained by fitting the online pH profile using nonlinear least square optimization method

	Temperature (°C)	Rate constant k (10^{-5} L mol^{-1} s^{-1})	Apparent dissociation constants		
			pKb_{NH_2OH}	$pKa_{CH_3CONHOH}$	pKb_{NH_3}
Fitting Results	55	6.792 ± 0.710	7.001 ± 0.020	9.639 ± 0.014	4.814 ± 0.008
	50	3.827 ± 0.322	7.010 ± 0.012	9.726 ± 0.108	4.839 ± 0.086
	45	2.134 ± 0.235	7.045 ± 0.024	9.690 ± 0.007	4.748 ± 0.006
	40	1.451 ± 0.195	7.071 ± 0.026	9.702 ± 0.107	4.784 ± 0.068
	35	0.894 ± 0.108	7.090 ± 0.055	9.753 ± 0.075	4.839 ± 0.058
Literature	25	–	8.060[a]	9.370[b]	4.750[a]

[a]Reference [35]

[b]Reference [45]

Table 3 Evaluated values of rate constant k and apparent dissociation constants of substances at different temperatures obtained by simultaneously fitting the online IR spectra and pH profile using multi-objective fitting method

Temperature (°C)	Rate constant k (10^{-5} L mol^{-1} s^{-1})	Apparent dissociation constants		
		pKb_{NH_2OH}	$pKa_{CH_3CONHOH}$	pKb_{NH_3}
55	6.314 ± 0.009	6.997 ± 0.008	9.598 ± 0.110	4.775 ± 0.084
50	3.520 ± 0.002	6.988 ± 0.028	9.687 ± 0.038	4.806 ± 0.027
45	2.308 ± 0.132	7.059 ± 0.014	9.754 ± 0.185	4.815 ± 0.129
40	1.495 ± 0.004	7.101 ± 0.087	9.671 ± 0.115	4.773 ± 0.079
35	0.804 ± 0.018	7.064 ± 0.035	9.622 ± 0.110	4.722 ± 0.087

Fitting results of single-objective fitting

Fitting results of online IR spectra

Before fitting the online infrared spectra to evaluate kinetic parameters, the applicability of the Beer-Lambert law was validated within the concentration range of 0.5–5 mol L^{-1} for the relevant substances. This validation process ensures the feasibility of the parameter evaluation method based on the Beer-Lambert law. See Supplementary Information for more details.

As mentioned above, to investigate the positive impact of introducing the similarity between the calculated spectra of components and the measured ones as additional physical constraints in the online infrared fitting, the online infrared data were additionally analyzed using two different methods: *A*) fitting without considering the measured spectra of components, i.e. traditional hard-modeling method, using Eq. 4 as the objective function, and *B*) directly replacing the corresponding rows of $\mathbf{S}_{calc}$ in Eq. 4 with the measured pure spectra in the fitting process. The main difference among the mentioned three methods is the objective function of the fitting process.

The evaluation results of the rate constants at different temperatures obtained by different methods are summarized in Table 1. Neither Method *A* nor *B* provided convincing values of *k* consistent with the pattern in Fig. 2, which shows that the reaction rate increases with the temperature. Compared with them, the evaluation results obtained by introducing the similarity between the calculated spectra and the measured pure ones into the objective function of the fitting process (Method *C*) are more reasonable. Further details can be found in the Supplementary Information.

Fig. 3 shows the comparison between the modeling results and experimental measurements. By using the online infrared spectra from a single experiment conducted at 55 °C as the fitting object, and Eq. 5 as the objective function, the evaluation value of *k* and the calculated infrared spectra of the reaction process can be obtained. Fig. 3a shows the comparison between the calculated and measured absorbance values at corresponding wavenumbers, indicating a good fit and confirming that the reaction can be described by the second-order kinetic model developed in this study. Fig. 3b shows the corresponding calculated pure spectra (solid lines)

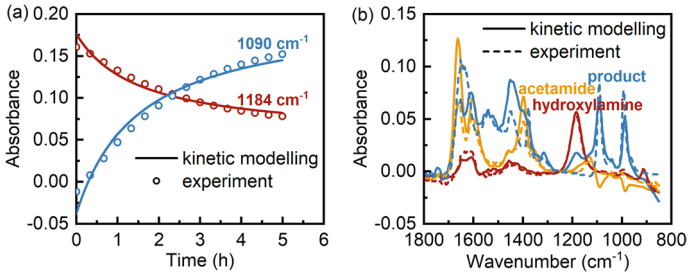

Fig. 3 **a** Solid lines: the absorbance-time profiles calculated by the kinetic model (Eq. 1), where the value of rate constant *k* was evaluated by fitting the online IR spectra at 55 °C using Eq. 5; points: the absorbance-time profiles measured by the online IR spectrometer at 55 °C; **b** Solid lines: spectra of substances calculated by kinetic model; dashed lines: measured spectra of pure substances

obtained by Eq. 3 compared to the measured spectra of pure substances (dashed lines), which are in good consistency at the peak positions.

Fitting results of online pH profile

The evaluation results of the rate constant at different temperatures obtained from the online pH profile fitting are summarized in Table 2. In addition to the rate constant k, the fitting results of online pH profile also include the evaluation values of apparent dissociation constants, as shown in Table 2, where pKb_{NH_2OH},$pKa_{CH_3CONHOH}$ and pKb_{NH_3} are the negative logarithms (base 10) of Kb_{NH_2OH},$Ka_{CH_3CONHOH}$ and Kb_{NH_3}.

Fig. 4 shows the comparison between the modeling result and experimental measurement. By using the pH data from a single experiment conducted at 55 °C as the fitting object, the evaluation value of k and the calculated pH of the reaction process can be obtained. It can be seen from Fig. 4 that the calculated result shows good consistency with online measured pH profile.

In the pH fitting process, the simulation equation of pH was simplified by neglecting the influence of the activity coefficient of each component on the dissociation constant. The fitting results shows that such simplification has no great influence on the fitting results of rate constants. However, the obtained dissociation constants exhibit inconsistencies compared to those reported in the literature, possibly due to variations in temperature and changes in the activity coefficient caused by stronger ionic strength in high concentration solutions. Therefore, we refer to the dissociation constants we used in Eq. 14 as apparent dissociation constants, which actually represent the result of combining the activity coefficient and the actual dissociation constants [37].

Fitting results of multi-objective fitting

Fig. 5 shows the Pareto frontier calculated by NSGA-II, using both IR spectra and pH data from a single experiment conducted at 55 °C as the fitting objects. The final optimal solution determined by WSM is highlighted. Specific parameter evaluation results corresponding to the Pareto frontier are summarized in Table S4. Note that since pH is one of the fitting objects, the multi-objective fitting also provided the evaluations of the apparent dissociation constants as additional results. Table S4 also shows the scores of each group of solutions calculated by WSM, and the solution

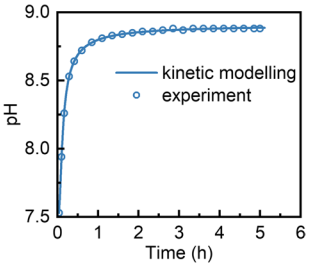

Fig. 4 Solid line: the pH-time profile calculated by the kinetic model, where the value of rate constant k was evaluated by fitting the online pH profile at 55 °C using nonlinear least square optimization method; points: the pH-time profiles measured by online pH probe at 55 °C

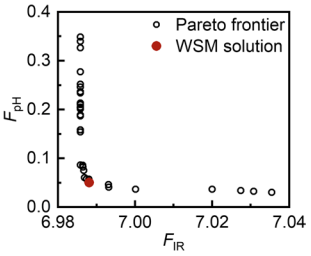

Fig. 5 Pareto frontier obtained by simultaneously fitting the online IR spectra and pH profile of a single experiment at 55 °C using NSGA-II, and the final optimal solution selected by WSM

with the highest score was automatically selected as the final solution for multi-objective fitting.

The evaluation results at different temperatures obtained by the multi-objective fitting method are summarized in Table 3. From the standard deviation of the rate constant evaluation results at each temperature, it can be seen that the results of multi-objective fitting exhibit high stability.

Comparison between different fitting methods

The logarithms (base e) of the rate constant evaluation results at different temperatures using the mentioned three different fitting methods were subjected to linear regression. The linear regression results are shown in Fig. 6. The evaluation values of activation energy and pre-exponential factor derived from the slope and intercept of the regression lines, and the coefficient of determination (R^2) for each regression line are shown in Table 4.

It can be seen that ln$k$ obtained from both infrared and pH data fitting have good linear relationships with $1/T$, as shown by their R^2 values (0.994 and 0.992). The regression lines obtained by these two methods are highly coincident, indicating that

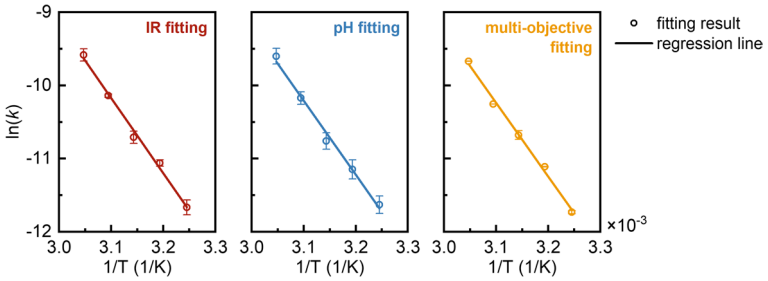

Fig. 6 Linear regression of ln(k) against $1/T$. Points represent the average of the parameter evaluation results at the same temperature, and error bars were determined from the standard deviation

Table 4 Evaluated values of activation energy E_A and pre-exponential factor A

	E_A (kJ mol^{-1})	ln(A)	R^2
IR fitting	85.096 ± 3.909	21.556 ± 1.478	0.994
pH fitting	84.476 ± 4.479	21.289 ± 1.694	0.992
multi-objective fitting	83.719 ± 3.373	20.976 ± 1.276	0.995

although online pH probe can provide less data than online infrared spectroscopy, the amount of online pH data is enough to support the kinetic analysis of a complete reaction process, and the kinetic fitting of pH data shows a good agreement with the infrared fitting result. However, it can be seen from the standard deviations in Table 2 and the error bars in Fig. 6 that despite the high reproducibility of pH data obtained from multiple repeated experiments, the parameter evaluation values may still exhibit noticeable instability. This may be attributed to the smaller data amount of pH measurement and more model parameters involved.

Regarding the multi-objective fitting results, the R^2 of the regression line increases to 0.995, and the relative standard deviation of the rate constant k evaluated through this method is the smallest among the three methods (maximum 5.719%). This improvement demonstrates its potential to take full advantage of the complementary information provided by the two online sensors and reduce the deviation in parameter evaluation results caused by measurement errors from a single instrument, leading to more accurate and stable kinetic parameter evaluation results.

Conclusions

In this study, the online infrared spectra and pH profile were separately used as fitting objects to evaluate the kinetic parameters of the acetohydroxamic acid synthesis reaction, including the rate constant and the activation energy. A multi-objective fitting method was further utilized to evaluate both online data simultaneously. The fitting results of kinetic parameters obtained by these three methods were close, which demonstrated the credibility of the results.

The infrared spectra data of the reaction process is extensive and contains abundant information, but the kinetic fitting based on online infrared spectra is easily affected by the rotational ambiguity, and even if the calculated concentrations have been forced to conform to the kinetic model, the wrong result may still be obtained. In this study, the similarity between the calculated spectrum and the measured pure one of each substance was introduced as an additional physical constraint, and the obtained fitting results showed that the rotational ambiguity was well restrained.

Regarding the fitting of pH data, the apparent dissociation constants of the weak acidic and basic substances participating in the reaction were also evaluated as additional results through the fitting process of the pH profile. However, the amount of pH data is significantly smaller than the infrared spectra data, making the accuracy of parameter evaluation based on pH data fitting easily influenced by the measurement precision of the pH probe.

The above limitations of kinetic parameter evaluation based on single fitting object can be easily overcome through multi-objective fitting. Monitoring a reaction with multiple instruments enables the acquisition of diverse data and supplementary information about the reaction. By considering the tradeoff between the fitting of different experimental data, the multi-objective fitting method has more chance to lead to reasonable and steady results. Therefore, the multi-instrument measurement in the experimental process and multi-instrumental data analysis in

the same time can become one of the effective directions to improve the accuracy of the kinetic parameter evaluation results.

Supplementary Information The online version contains supplementary material available at https://doi.org/10.1007/s11144-023-02465-1.

Funding This work was supported by National Natural Science Foundation of China (Grant numbers 62103391 and 22173087).

Data availability The datasets analyzed during the current study are available from the corresponding author on reasonable request.

Declarations

Competing interests The authors have no relevant financial or non-financial interests to disclose.

References

1. Sánchez-García I, Bonales LJ, Galán H et al (2019) Spectroscopic study of acetohydroxamic acid (AHA) hydrolysis in the presence of europium. implications in the extraction system studies for lanthanide and actinide separation. New J Chem 43:15714–15722. https://doi.org/10.1039/C9NJ03360B
2. Bracher BH, Small RWH (1970) The crystal structure of acetohydroxamic acid hemihydrate. Acta Crystallogr B Struct Sci 26:1705–1709. https://doi.org/10.1107/S0567740870004764
3. LeBlond C, Wang J, Larsen R, Orella C, Sun Y-K (1998) A combined approach to characterization of catalytic reactions using in situ kinetic probes. Top Catal 5:149–158. https://doi.org/10.1023/A:1019149919423
4. Blackmond DG (2005) Reaction progress kinetic analysis: a powerful methodology for mechanistic studies of complex catalytic reactions. Angew Chem Int Ed 44:4302–4320. https://doi.org/10.1002/anie.200462544
5. Tomazett VK, Santos WG, Lima-Neto BS (2017) Infrared spectroscopy as an effective tool in ring-opening metathesis polymerization: monitoring the polymerization kinetics of norbornene with amine-based Ru catalysts in real time. Reac Kinet Mech Cat 120:663–672. https://doi.org/10.1007/s11144-017-1147-5
6. Liu Y-C, Huang A-C, Tang Y et al (2022) Thermokinetic analysis of the stability of acetic anhydride hydrolysis in isothermal calorimetry techniques. J Therm Anal Calorim 147:7865–7873. https://doi.org/10.1007/s10973-021-11065-x
7. Bezemer E, Rutan S (2002) Resolution of overlapped NMR spectra by two-way multivariate curve resolution alternating least squares with imbedded kinetic fitting. Anal Chim Acta 459:277–289. https://doi.org/10.1016/S0003-2670(02)00116-2
8. Schwolow S, Braun F, Rädle M et al (2015) Fast and efficient acquisition of kinetic data in microreactors using in-line Raman analysis. Org Process Res Dev 19:1286–1292. https://doi.org/10.1021/acs.oprd.5b00184
9. Zakarianezhad M, Habibi-Khorassani M, Khajehali Z et al (2014) Mechanistic investigation of the reaction between triphenylphosphine, dialkyl acetylenedicarboxylates and pyridazinone: a theoretical, NMR and kinetic study. Reac Kinet Mech Cat 111:461–474. https://doi.org/10.1007/s11144-013-0653-3
10. Chung R, Hein JE (2017) The more, the better: simultaneous in situ reaction monitoring provides rapid mechanistic and kinetic insight. Top Catal 60:594–608. https://doi.org/10.1007/s11244-017-0737-9
11. Marcel M, Zuberbuehler AD (1990) Nonlinear least-squares fitting of multivariate absorption data. Anal Chem 62:2220–2224. https://doi.org/10.1021/ac00219a013

12. Bugnon P, Chottard J-C, Jestin J-L, Jung B, Laurenczy G, Maeder M, Merbach AE, Zuberbühler AD (1994) Second-order globalisation for the determination of activation parameters in kinetics. Anal Chim Acta 298:193–201. https://doi.org/10.1016/0003-2670(94)00255-X
13. de Juan A, MaederMartínezTauler MMR (2000) Combining hard- and soft-modelling to solve kinetic problems. Chemom Intell Lab Syst 54:123–141. https://doi.org/10.1016/S0169-7439(00)00112-X
14. Fath V, Lau P, Greve C, Kockmann N, Röder T (2020) Efficient kinetic data acquisition and model prediction: continuous flow microreactors, inline fourier transform infrared spectroscopy, and self-modeling curve resolution. Org Process Res Dev 24:1955–1968. https://doi.org/10.1021/acs.oprd.0c00037
15. Zogg A, Fischer U, Hungerbühler K (2004) A new approach for a combined evaluation of calorimetric and online infrared data to identify kinetic and thermodynamic parameters of a chemical reaction. Chemom Intell Lab Syst 71:165–176. https://doi.org/10.1016/j.chemolab.2004.01.025
16. de Juan A, Tauler R (2003) Chemometrics applied to unravel multicomponent processes and mixtures. Anal Chim Acta 500:195–210. https://doi.org/10.1016/S0003-2670(03)00724-4
17. Tauler R, Smilde A, Kowalski B (1995) Selectivity, local rank, three-way data analysis and ambiguity in multivariate curve resolution. J Chemom 9:31–58. https://doi.org/10.1002/cem.1180090105
18. Carvalho A, Sanchez M, Wattoom J, Brereton R (2006) Comparison of PLS and kinetic models for a second-order reaction as monitored using ultraviolet visible and mid-infrared spectroscopy. Talanta 68:1190–1200. https://doi.org/10.1016/j.talanta.2005.07.053
19. Chung R, Yu D, Thai VT et al (2015) Tandem reaction progress analysis as a means for dissecting catalytic reactions: Application to the aza-Piancatelli rearrangement. ACS Catal 5:4579–4585. https://doi.org/10.1021/acscatal.5b01087
20. Deb K, Pratap A, Agarwal S, Meyarivan T (2002) A fast and elitist multiobjective genetic algorithm: NSGA-II. IEEE Trans Evol Computat 6:182–197. https://doi.org/10.1109/4235.996017
21. Syed Z, Sogani M (2022). In: Arora S, Kumar A, Ogita S, Yau Y-Y (eds) Innovations in environmental biotechnology. Singapore Nature, Singapore
22. Jencks WP, Mary G (1964) The reaction of hydroxylamine with amides. Kinetic evidence for the existence of a tetrahedral addition intermediate. J Am Chem Soc 86:5616–5620. https://doi.org/10.1021/ja01078a042
23. Tsu J, Díaz VHG, Willis MJ (2019) Computational approaches to kinetic model selection. Comput Chem Eng 121:618–632. https://doi.org/10.1016/j.compchemeng.2018.12.002
24. de Juan A, Jaumot J, Tauler R (2014) Multivariate curve resolution (MCR). Solving the mixture analysis problem. Anal Methods 6:4964–4976. https://doi.org/10.1039/C4AY00571F
25. de Juan A, Maeder M, Martínez M, Tauler R, (2001) Application of a novel resolution approach combining soft- and hard-modelling features to investigate temperature-dependent kinetic processes. Anal Chim Acta 442:337–350. https://doi.org/10.1016/S0003-2670(01)01181-3
26. Gampp H, Maeder M, J. Meyer C, D. Zuberbuehler A, (1987) Quantification of a known component in an unknown mixture. Anal Chim Acta 193:287–293. https://doi.org/10.1016/S0003-2670(00)86160-7
27. Bijlsma S, Smilde AK (2000) Estimating reaction rate constants from a two-step reaction: a comparison between two-way and three-way methods. J Chemom 14:541–560. https://doi.org/10.1002/1099-128X(200009/12)14:5/6%3c541::AID-CEM609%3e3.0.CO;2-1
28. Scott Barney G (1976) A kinetic study of the reaction of plutonium(IV) with hydroxylamine. J Inorg Nucl Chem 38:1677–1681. https://doi.org/10.1016/0022-1902(76)80660-4
29. Monzyk B, Crumbliss AL (1980) Acid dissociation constants (Ka) and their temperature dependencies (ΔHa, ΔSa) for a series of carbon- and nitrogen-substituted hydroxamic acids in aqueous solution. J Org Chem 45:4670–4675. https://doi.org/10.1021/jo01311a024
30. Max J-J, Chapados C (2013) Aqueous ammonia and ammonium chloride hydrates: principal infrared spectra. J Mol Struct 1046:124–135. https://doi.org/10.1016/j.molstruc.2013.04.045
31. Boyd CE, Tucker CS, Viriyatum R (2011) Interpretation of pH, acidity, and alkalinity in aquaculture and fisheries. N Am J Aqualcult 73:403–408. https://doi.org/10.1080/15222055.2011.620861
32. Angelidaki I, Ellegaard L, Ahring BK (1993) A mathematical model for dynamic simulation of anaerobic digestion of complex substrates: focusing on ammonia inhibition. Biotechnol Bioeng 42:159–166. https://doi.org/10.1002/bit.260420203
33. Campos E, Flotats X (2003) Dynamic simulation of pH in anaerobic processes. Appl Biochem Biotechnol 109:63–76. https://doi.org/10.1385/ABAB:109:1-3:63

34. Magrí A, Ll C, López H, Campos E, Balaguer M, Colprim J, Flotats X (2007) A model for the simulation of the SHARON process: pH as a key factor. Environ Technol 28:255–265. https://doi.org/10.1080/09593332808618791
35. Rumble JR (2022) CRC handbook of chemistry and physics: A ready-reference book of chemical and physical data, 103rd edn. CRC Press, London
36. Sommer SG, Husted S (1995) A simple model of pH in slurry. J Agric Sci 124:447–453. https://doi.org/10.1017/S0021859600073408
37. Phosphate Buffer Issues. https://www.chem.fsu.edu/chemlab/Mastering/PhosphateBuffers.htm. Accessed 16 Mar 2023
38. Deb K (2011). In: Wang L, Ng A, Deb K (eds) Multi-objective evolutionary optimisation for product design and manufacturing. Springer, London
39. Soleimani S, Eckels S (2022) Multi-objective optimization of 3D micro-fins using NSGA-II. Int J Heat Mass Transfer 197:123315. https://doi.org/10.1016/j.ijheatmasstransfer.2022.123315
40. Jafaryeganeh H, Ventura M, Guedes Soares C (2020) Application of multi-criteria decision making methods for selection of ship internal layout design from a Pareto optimal set. Ocean Eng 202:107151. https://doi.org/10.1016/j.oceaneng.2020.107151
41. Jafaryeganeh H, Ventura M, Guedes Soares C (2020) Effect of normalization techniques in multi-criteria decision making methods for the design of ship internal layout from a Pareto optimal set. Struct Multidisc Optim 62:1849–1863. https://doi.org/10.1007/s00158-020-02581-9
42. Laidler KJ (1984) The development of the Arrhenius equation. J Chem Educ 61:494. https://doi.org/10.1021/ed061p494
43. Makarewicz J, Kręglewski M, Senent ML (1997) Ab initio potential energy surface and internal torsional–wagging states of hydroxylamine. J Mol Spectrosc 186:162–170. https://doi.org/10.1006/jmsp.1997.7425
44. Edwards DC, Nielsen SB, Jarzęcki AA, Spiro TG, Myneni S (2005) Experimental and theoretical vibrational spectroscopy studies of acetohydroxamic acid and desferrioxamine B in aqueous solution: Effects of pH and iron complexation. Geochim Cosmochim Acta 69:3237–3248. https://doi.org/10.1016/j.gca.2005.01.030
45. Schwarzenbach G, Schwarzenbach K (1963) Hydroxamatkomplexe I. die Stabilität der Eisen(III)-Komplexe einfacher Hydroxamsäuren und des Ferrioxamins B. Helv Chim Acta 46:1390–1400. https://doi.org/10.1002/hlca.19630460434